Supporting Information

High performance and low cost organic solar cells based on pentacyclic A-DA′D-A acceptor with efficiency over 16%

Xiang Xu[a], Qingya Wei[a], Jiage Song[a], Jianhua Jing[b], Yanwei Chen [b], Fei Huang[b], Xinhui Lu[c], Yonghua Zhou[a], Jun Yuan [a] and Yingping Zou [a*]

a. College of Chemistry and Chemical Engineering, Central South University, Changsha 410083, China

b. State Key Laboratory of Luminescent Materials and Devices, Institute of Polymer Optoelectronic Materials and Devices, School of Materials Science and Engineering, South China University of Technology, 381 Wushan Road, Guangzhou 510640, China

c. Department of Physics, The Chinese University of Hong Kong, New Territories, Hong Kong 999077, China

1.1 Device measurement and characterization

The current density–voltage (J-V) characteristics of the devices were measured under 100 mW/cm^2 air mass, AM 1.5 G spectra with a solar simulator (SS-F5, Enlitech). Light intensity was calibrated prior to performance measurement using a silicon photodiode with a KG5 filter approved by the National Renewable Energy Laboratory. The EQE spectra measurements were performed on a commercial EQE measurement system (QE-R3011, Enlitech). Light intensity-dependent V_{oc} and J_{sc} measurements were performed using the J-V measurement system, and the light intensity was varied from 0.1 sun to 1 sun. The active area of the devices was typically 5 mm^2.

Transient photocurrent (TPC) measurements were carried out by photoexciting the OSC devices with an attenuated 580 nm laser pulse. The pulse had a 120 fs width. Tektronix TDS 3052C digitizing oscilloscope with an input impedance of 50 X at the short circuit state was used to serially connect the sealed devices after excitation, and data was recorded. A similar setup to that used for photocurrent measurements was used for transient photovoltage (TPV) measurements, and the devices were connected to an oscilloscope using a 1 MX input impedance at the open-circuit state. The laser pulse caused photovoltage perturbation was less than 5% of the V_{oc} produced by the specified background illumination intensity, which was 0.7 suns of background illumination.

Space charge limited current (SCLC) measurements: The structure of hole-only devices was Glass/ITO/PEDOT: PSS/BHJ/MoO_x (10 nm)/Ag (100 nm). The structure of electron-only devices was Glass/ITO/ZnO/BHJ/ PDINN (5 nm)/Ag (100 nm). The mobility was estimated by fitting the dark current to the single-carrier SCLC model, which is expressed by the equation $J = (9/8)\varepsilon_0\varepsilon_r\mu((V^2)/(d^3))$, where J is the current density, μ is the zero-field mobility, ε_0 is the permittivity of free space, ε_r is the relative permittivity of the material, d is the thickness of the active layers, and

V is the effective voltage. The effective voltage was obtained by subtracting the built-in voltage (V_{bi}) and the voltage drop (V_s) from the series resistance of the whole device except for the active layers from the applied voltage (V_{appl}), $V = V_{appl} - V_{bi} - V_s$. The mobility can be calculated from the slope of the $J^{1/2}$-V curves.

A grazing incidence wide-angle X-ray scattering (GIWAXS) study was performed using the small-angle and wide-angle X-ray scattering beamlines. In the integration mode, a Pilatus 1M two-dimensional detector with active pixels of 0.172 mm × 0.172 mm was employed. About 300 mm downstream from the sample site, the detector was placed. A silver behenate standard was used to calculate the precise sample to detector distance. To create a suitably large q space, an incident X-ray with an energy of 11 keV and a spot size of 0.25 mm × 0.1 mm was utilized. A modified version of Nika was used to reduce and analyze the two-dimensional raw data. The provided GIWAXS patterns were adjusted to take into account the missing wedge and represent the actual Qz and Qxy axes. The sample scattering's maximum intensity and the bottom layer scattering's minimal contribution were used to calculate the critical incident angle. The incident X-ray was transformed into an evanescent wave that traveled over the upper surface of the thin films due to the shallow incidence angle scattering, which was measured at 0.02°.

CE and TPV measurements: Monitoring the photovoltage decay upon a modest optical disturbance at various constant bias light-intensity conditions provided the basis for the TPV approach employing PAIOS (using the same white LED for TPC measurements and under open-circuit condition). A variety of V_{OC} s can be examined as a result of variable bias light intensity. There was a slight optical disturbance used (<3% of the V_{OC}, so that $\Delta V_{OC} \ll V_{OC}$). It was therefore possible to directly see nongeminate charge carrier recombination by recording the voltage decrease that followed. All devices' photovoltage decay kinetics exhibit a mono-exponential decay, as shown by the equation: $\delta V = A\exp(-t/\tau)$, where t is the time and τ is the charge carrier lifetime. Under open-circuit voltage conditions, the charge carrier density n was measured using the CE method. The device maintained an open circuit and was illuminated. The voltage was reduced to zero or taken to a short-circuit condition within a few hundred nanoseconds after the light was switched out in order to extract the charges. The current was integrated to determine how many extracted charges there were. The charge carrier lives and charge carrier densities may be plotted using the charge carrier lifetime acquired from TPV and the charge carrier density obtained from CE. A power-law connection exists between the charge carrier lifetime and charge density: $\tau = \tau_0\, n^{-\lambda}$. The nongeminate recombination constant k_{rec} was then inferred from the carrier lifetimes and densities according to $k_{rec} = 1/(\lambda + 1)n\tau$, where λ is the recombination order determined from Figure 5e.

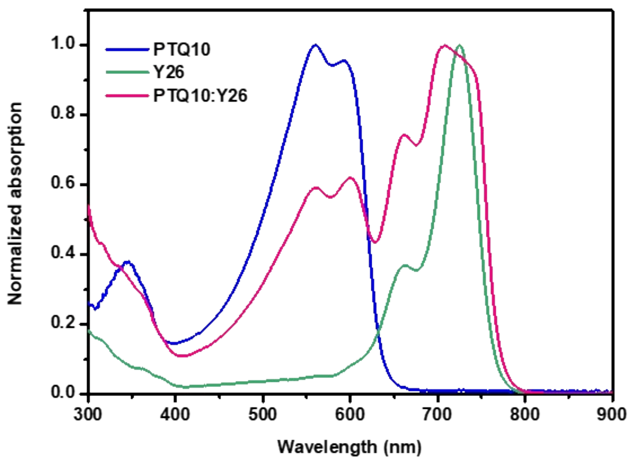

Figure S1. The normalized absorption of PTQ10, Y26, and PTQ10:Y26 in CF solution.

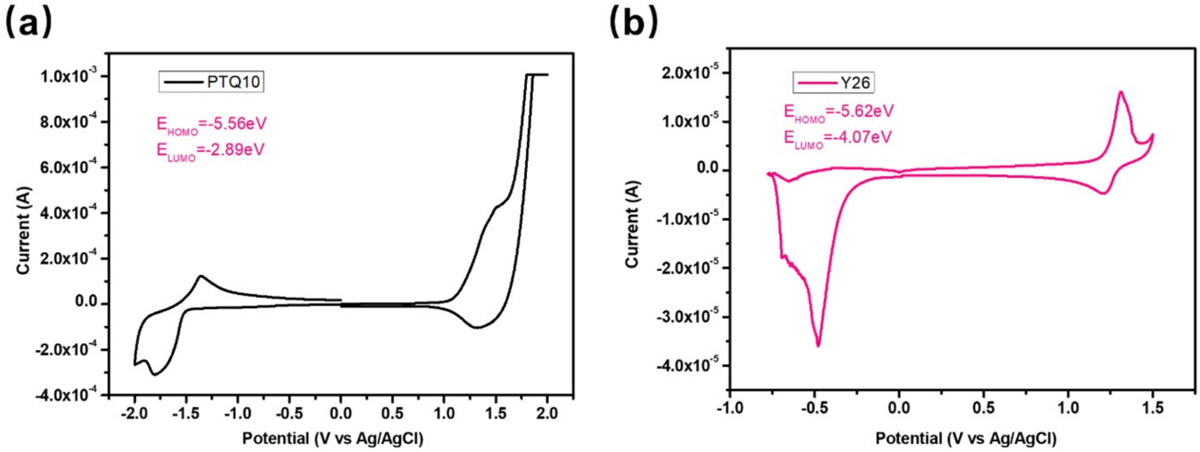

Figure S2.Cyclic voltammetry (CV) curves of PTQ10 and Y26.

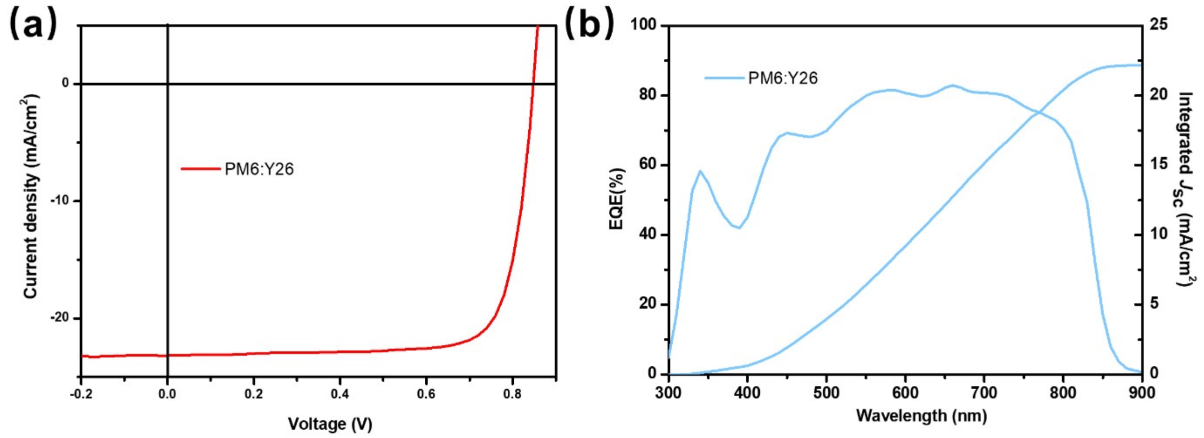

Figure S3. (a) The J-V curve and (b) EQE spectrum and its corresponding integrated J_{sc} of PM6:Y26 OSCs.

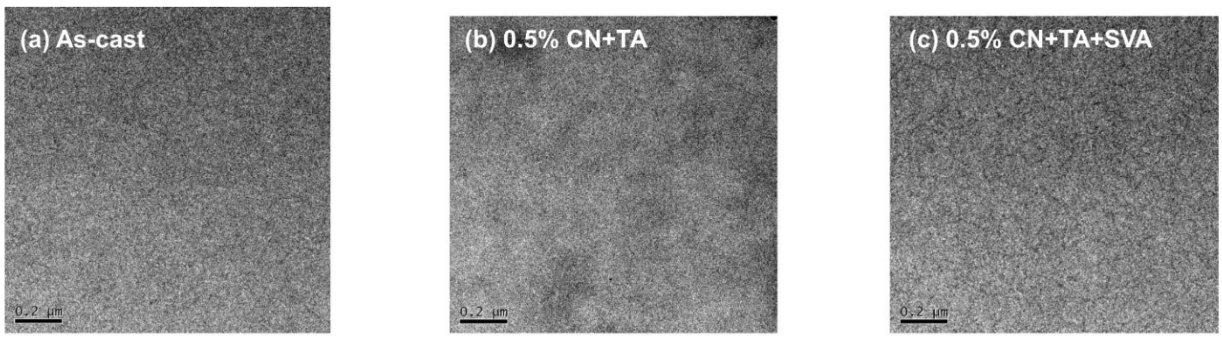

Figure S4. The TEM images of PTQ10:Y26 films with different treatments.

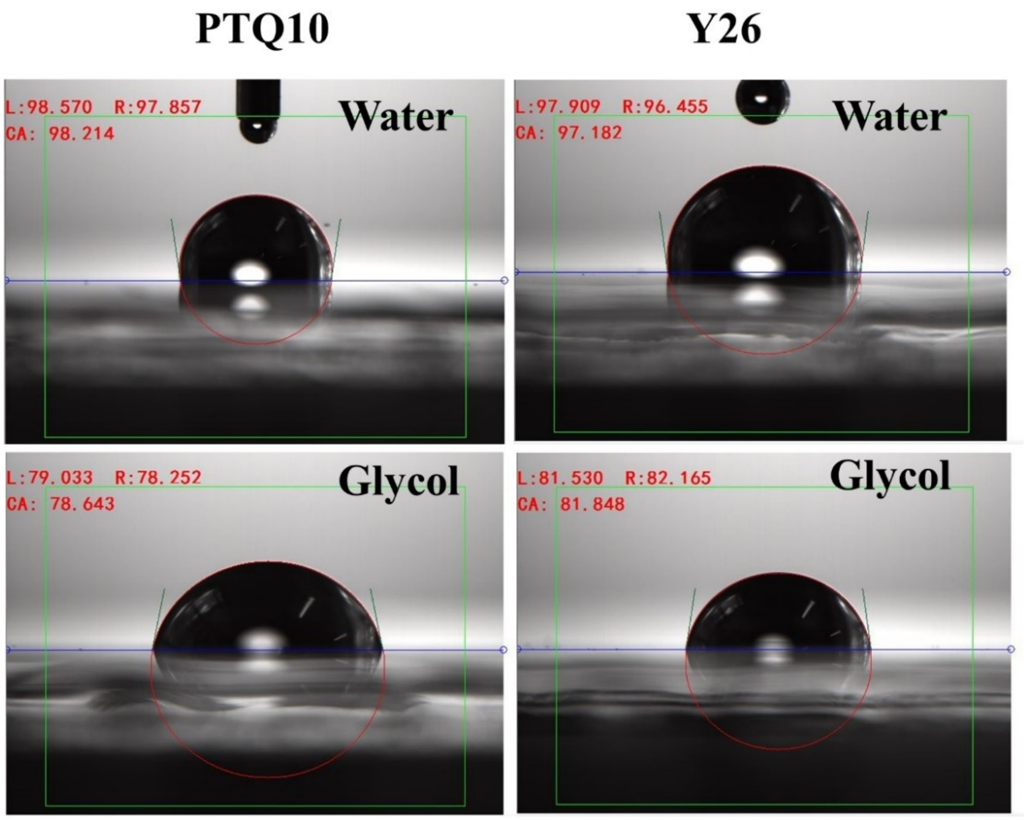

Figure S5. The contact angle measured by using water and glycol as wetting liquids.

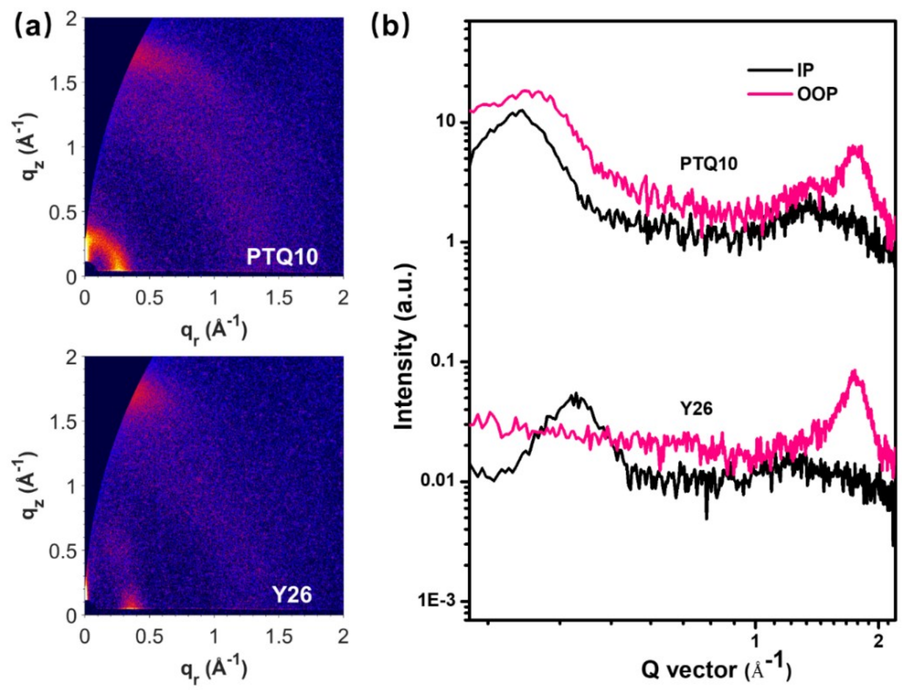

Figure S6. (a) GIWAXS scattering patterns and (b) the corresponding profiles for the pristine PTQ10 and Y26 films.

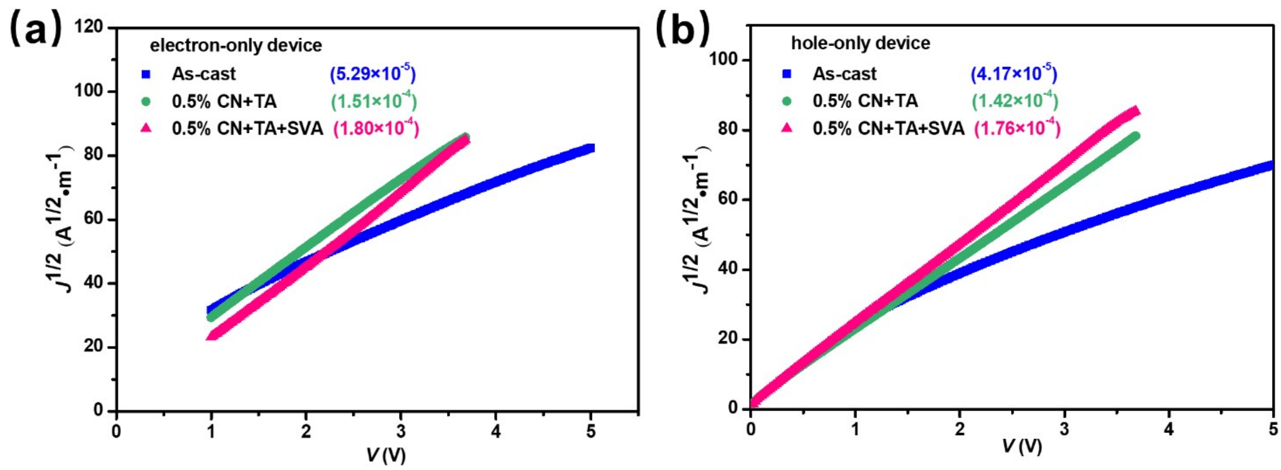

Figure S7. (a) Electron mobility and (b) Hole mobility of the studied devices measured by SCLC method.

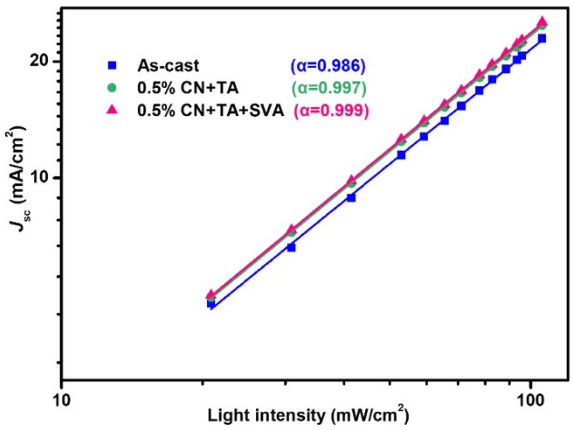

Figure S8. Light intensity dependence of J_{sc} for binary PTQ10:Y26 devices under different treatment conditions.

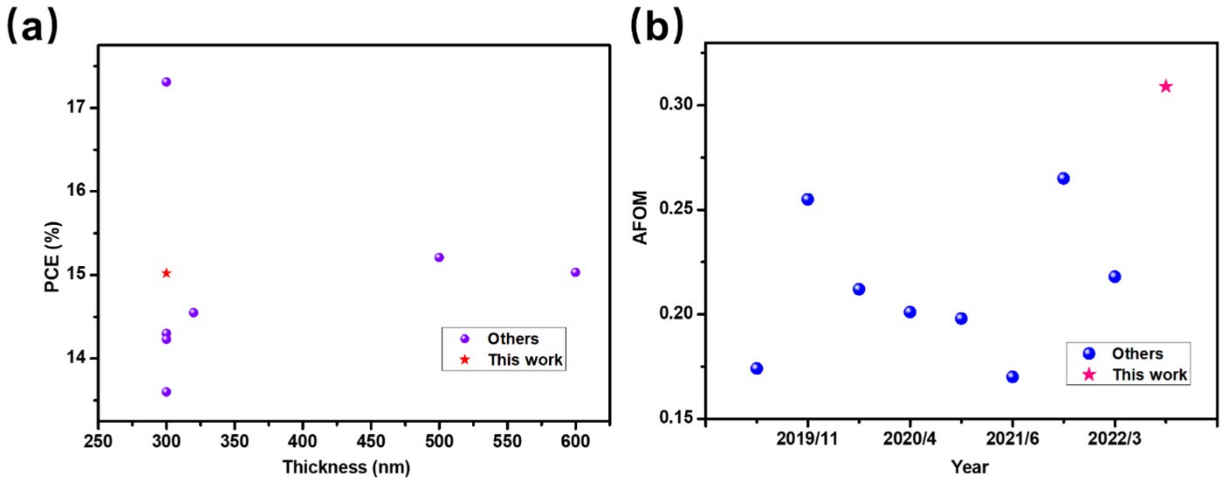

Figure S9. (a) Summary of the reported thick-film OSCs in recent years. (b) The AFOM values of some classic systems that based on A-DA′D-A acceptors.

Table S1. The photovoltaic performance of PTQ10:Y26 with different SVA time.

BHJ	SVA time	V_{oc} (V)	J_{sc} (mA cm^{-2})	FF (%)	PCE (%)
PTQ10:Y26	0 min	0.88	22.56	76.27	15.23
	2 min	0.89	23.08	76.14	15.66
	5 min	0.89	23.57	76.73	16.01
	7 min	0.89	22.61	77.05	15.51
	10 min	0.89	22.77	76.34	15.49

Table S2. The photovoltaic performance of PM6:Y26 with different treatments.

BHJ		V_{oc} (V)	J_{sc} (mA cm^{-2})	FF (%)	PCE (%)
PM6:Y26	As-cast	0.872	21.72	74.80	14.17
	0.5%CN+TA	0.841	22.59	76.69	14.57
	0.5%CN+TA+SVA	0.848	23.17	78.64	15.44

Table S3. The photovoltaic performance of PTQ10:Y26 with different thickness.

BHJ		V_{oc} (V)	J_{sc} (mA cm^{-2})	FF (%)	PCE (%)
PTQ10:Y26	100 nm	0.89	23.57	76.73	16.01
	150 nm	0.89	23.14	75.79	15.55
	200 nm	0.88	23.20	75.52	15.45
	300 nm	0.88	23.34	73.30	15.02

Table S4. The summary of the thick-film OSCs based on A-DA′D-A acceptors in recent years.

BHJ	Thickness (nm)	V_{oc} (V)	J_{sc} (mA cm^{-2})	FF (%)	PCE (%)	Ref.
PM6:Y6	300	0.82	26.5	62.3	13.6	1
PM7:Y6:$PC_{71}BM$	300	0.802	26.8	66.7	14.3	2
PM6:Y6:BTP-M	300	0.855	26.87	62.06	14.23	3
Si25:Y14	430	0.782	26.82	73.38	15.39	4
Si25:Y14	600	0.782	28.50	67.46	15.03	4
PM6:BTP-eC9:L8-BO-F	300	0.836	28.36	73.0	17.31	5
PM6:BTP-eC9:L8-BO-F	500	0.835	27.49	66.4	15.21	5
PTQ10:Y26	300	0.88	23.34	73.30	15.02	This work

Table S5. The photovoltaic parameters of binary OSCs based on pentacyclic acceptors.

Donor: Acceptor	V_{OC} (V)	J_{SC} (mA cm^{-2})	FF (%)	PCE (%)	Ref
PDBT-T1: IC-C6IDT-IC	0.89	15.05	63	8.71	6
PDBT-T1: IC-C6IDT-IC	0.85	15.85	65	9.2	7
HFQx-T: BZIC	0.84	12.67	59	6.3	8
PBDB-T: IDT-N	0.79	15.88	71.91	9	9
PM6: IDTN	0.946	16.58	78	12.2	10
PBDB-T: NBDTP	0.937	15.72	66.4	10.1	11
PBDB-T: IDT-HN	0.93	14.43	76.41	10.22	12
FTAZ: IDIC	0.84	20.8	71.8	12.5	13
PTQ10: IDTPC	0.93	17.5	74.6	12.2	14
PBDB-T2Cl: IDIC-4Cl	0.83	16.21	68.69	9.24	15
FTAZ: IDIC1	0.896	13.6	58.5	7.13	16
BSFTR: NBDTP-F_{out}	0.797	21.69	70.93	12.26	17
PM6: DTP-C_{17}-4F	0.691	21.17	61.1	8.94	18
PTQ10: MO-IDIC	0.969	16.92	68.1	11.16	19
PTQ10: MO-IDIC-2F	0.906	19.87	74.8	13.46	19
PM6: IDIC-C4Ph	0.941	19.06	78.32	14.04	20
PM6: Y26	0.83	21.63	74.33	13.34	21
PTQ10:Y26	0.886	23.57	76.73	16.01	This work

1.2 Synthetic complexity (SC) calculation.

The SC is calculated by the equation as following:[22]

$$SC=35NSS/NSS_{max}+25\log(RY)/\log(RY_{max})+15NCC/NCC_{max}+15NUO/NUO_{max}+10NHC/NHC_{max}$$

Where NSS is the number of synthetic steps (NSS), RY is the reciprocal yields of the monomers, NUO is the number of unit operations required for the isolation/purification of the monomers, NCC is the number of column chromatographic purifications required by the monomers, and NHC is the number of hazardous chemicals used for their preparation. According to **Table S6**, values used for the normalization: NSS_{max} =17; RY_{max} = 33; NUO_{max} = 35; NCC_{max} = 9; NHC_{max} = 40.

Table S6. The absolute and normalized NSS, RY, NUO, NCC, and NHC and the corresponding SC of the relevant donor and acceptor materials in this work.

Materials	Absolute values					Normalized values					SC
	NSS	RY	NUO	NCC	NHC	NSS	RY	NUO	NCC	NHC	
P3HT[a)]	3	1.1	4	0	4	0.176	0.027	0.114	0	0.1	9.545
PM6[a)]	15	33	35	9	26	0.882	1	1	1	0.65	92.37
PM7[a)]	12	11.8	26	7	23	0.706	0.706	0.743	0.778	0.575	70.925
D18[a)]	17	25.64	27	9	40	1	0.928	0.771	1	1	94.765
P4T2F-HD[a)]	9	5.45	17	5	25	0.529	0.485	0.486	0.556	0.625	52.52
P5TCN-F25[b)]	12	6.67	19	5	28	0.706	0.542	0.543	0.556	0.7	61.745
PTQ10[a)]	7	3.11	14	1	16	0.412	0.325	0.4	0.111	0.4	34.21
Y6[a)]	17	25.5	29	6	30	1	0.926	0.829	0.667	0.75	88.09
Y6-BO[a)]	16	19.7	23	6	34	0.941	0.852	0.657	0.667	0.85	82.595
ZY-4Cl[a)]	13	15.55	20	5	32	0.765	0.784	0.571	0.556	0.8	71.28
Y26[c)]	14	7.156	19	6	22	0.823	0.563	0.543	0.667	0.55	66.53

a) The values of NSS, RY, NUO, NCC, and NHC were cited from Ref. 23. b) The values of NSS, RY, NUO, NCC, and NHC were cited from Ref. 24. c) The values of NSS, RY, NUO, NCC, and NHC were extracted from Ref.21.

References

1. J. Yuan, Y. Zhang, L. Zhou, G. Zhang, H.-L. Yip, T.-K. Lau, X. Lu, C. Zhu, H. Peng and P. A. Johnson, *Joule*, 2019, **3**, 1140-1151.
2. L. Ma, Y. Xu, Y. Zu, Q. Liao, B. Xu, C. An, S. Zhang and J. Hou, *Sci. China. Chem.*, 2020, **63**, 21-27.
3. L. Zhan, S. Li, T.-K. Lau, Y. Cui, X. Lu, M. Shi, C.-Z. Li, H. Li, J. Hou and H. Chen, *Energy Environ. Sci.*, 2020, **13**, 635-645.
4. F. Pan, M. Luo, X. Liu, H. Jiang, Z. Wang, D. Yuan, Q. Wang, L. Qing, Z. Zhang and L. Zhang, *J. Mater. Chem. A*, 2021, **9**, 7129-7136.
5. Y. Cai, Q. Li, G. Lu, H. S. Ryu, Y. Li, H. Jin, Z. Chen, Z. Tang, G. Lu, X. Hao, H. Y. Woo, C. Zhang and Y. Sun, *Nat. Commun.*, 2022, **13**, 2369.
6. Y. Lin, Q. He, F. Zhao, L. Huo, J. Mai, X. Lu, C.-J. Su, T. Li, J. Wang and J. Zhu, *J. Am. Chem. Soc.*, 2016, **138**, 2973-2976.
7. Y. Lin, T. Li, F. Zhao, L. Han, Z. Wang, Y. Wu, Q. He, J. Wang, L. Huo and Y. Sun, *Adv. Energy Mater.*, 2016, **6**, 1600854.
8. L. Feng, J. Yuan, Z. Zhang, H. Peng, Z.-G. Zhang, S. Xu, Y. Liu, Y. Li and Y. Zou, *ACS Appl. Mater. Interfaces*, 2017, **9**, 31985-31992.

9. R. Li, G. Liu, M. Xiao, X. Yang, X. Liu, Z. Wang, L. Ying, F. Huang and Y. Cao, *J. Mater. Chem. A*, 2017, **5**, 23926-23936.
10. S. Li, L. Ye, W. Zhao, X. Liu, J. Zhu, H. Ade and J. Hou, *Adv. Mater.*, 2017, **29**, 1704051.
11. H. Wu, H. Fan, S. Xu, C. Zhang, S. Chen, C. Yang, D. Chen, F. Liu and X. Zhu, *Solar RRL*, 2017, **1**, 1700165.
12. R. Li, G. Liu, R. Xie, Z. Wang, X. Yang, K. An, W. Zhong, X.-F. Jiang, L. Ying and F. Huang, *J. Mater. Chem. C*, 2018, **6**, 7046-7053.
13. Y. Lin, F. Zhao, S. K. Prasad, J. D. Chen, W. Cai, Q. Zhang, K. Chen, Y. Wu, W. Ma and F. Gao, *Adv. Mater.*, 2018, **30**, 1706363.
14. Z. Luo, C. Sun, S. Chen, Z.-G. Zhang, K. Wu, B. Qiu, C. Yang, Y. Li and C. Yang, *Adv. Energy Mater.*, 2018, **8**, 1800856.
15. J. Qu, H. Chen, J. Zhou, H. Lai, T. Liu, P. Chao, D. Li, Z. Xie, F. He and Y. Ma, *ACS Appl. Mater. Interfaces*, 2018, **10**, 39992-40000.
16. J. Zhu, Y. Wu, J. Rech, J. Wang, K. Liu, T. Li, Y. Lin, W. Ma, W. You and X. Zhan, *J. Mater. Chem. C*, 2018, **6**, 66-71.
17. H. Wu, Q. Yue, Z. Zhou, S. Chen, D. Zhang, S. Xu, H. Zhou, C. Yang, H. Fan and X. Zhu, *J. Mater. Chem. A*, 2019, **7**, 15944-15950.
18. X. Chen, H. Liu, L. Xia, T. Hayat, A. Alsaedi and Z. a. Tan, *Chem. Commun.*, 2019, **55**, 7057-7060.
19. X. Li, F. Pan, C. Sun, M. Zhang, Z. Wang, J. Du, J. Wang, M. Xiao, L. Xue and Z.-G. Zhang, *Nat. Commun.*, 2019, **10**, 1-11.
20. Y. Li, N. Zheng, L. Yu, S. Wen, C. Gao, M. Sun and R. Yang, *Adv. Mater.*, 2019, **31**, 1807832.
21. J. Song, F. Cai, C. Zhu, H. Chen, Q. Wei, D. Li, C. Zhang, R. Zhang, J. Yuan, H. Peng, S. K. So and Y. Zou, *Solar RRL*, 2021, **5**, 2100281.
22. R. Po, G. Bianchi, C. Carbonera and A. Pellegrino, *Macromolecules*, 2015, **48**, 453-461.
23. J. Xiao, X. e. Jia, C. Duan, F. Huang, H.-L. Yip and Y. Cao, *Adv. Mater.*, 2021, **33**, 2008158.
24. X. Yuan, Y. Zhao, D. Xie, L. Pan, X. Liu, C. Duan, F. Huang and Y. Cao, *Joule*, 2022, **6**, 647-661.